

SEARCH FOR BLAZAR FLUX-CORRELATED TEV NEUTRINOS IN ICECUBE 40-STRING DATA

C. F. TURLEY^{1,3,5}, D. B. FOX^{2,3,4}, K. MURASE^{1,2,3,4}, A. FALCONE^{2,3}, M. BARNABA², S. COUTU^{1,3}, D. F. COWEN^{1,2,3},
G. FILIPPATOS^{1,3}, C. HANNA^{1,2,3}, A. KEIVANI^{1,3}, C. MESSICK^{1,3}, P. MÉSZÁROS^{1,2,3,4}, M. MOSTAFÁ^{1,2,3},
F. OIKONOMOU^{1,3}, I. SHOEMAKER^{1,3}, M. TOOMEY^{1,3}, G. TEŠIĆ^{1,3}
(THE AMON CORE TEAM)

¹Department of Physics, Pennsylvania State University, University Park, PA 16802, USA

²Department of Astronomy & Astrophysics, Pennsylvania State University, University Park, PA 16802, USA

³Center for Particle & Gravitational Astrophysics, Institute for Gravitation and the Cosmos, Pennsylvania State University, University Park, PA 16802, USA

⁴Center for Theoretical & Observational Cosmology, Institute for Gravitation and the Cosmos, Pennsylvania State University, University Park, PA 16802, USA

⁵cft114@psu.edu

ABSTRACT

We present a targeted search for blazar flux-correlated high-energy ($\varepsilon_\nu \gtrsim 1$ TeV) neutrinos from six bright northern blazars, using the public database of northern-hemisphere neutrinos detected during “IC40” 40-string operations of the IceCube neutrino observatory (April 2008 to May 2009). Our six targeted blazars are subjects of long-term monitoring campaigns by the VERITAS TeV γ -ray observatory. We use the publicly-available VERITAS lightcurves to identify periods of excess and flaring emission. These predefined intervals serve as our “active temporal windows” in a search for an excess of neutrinos, relative to Poisson fluctuations of the near-isotropic atmospheric neutrino background which dominates at these energies. After defining the parameters of an optimized search, we confirm the expected Poisson behavior with Monte Carlo simulations prior to testing for excess neutrinos in the actual data. We make two searches: One for excess neutrinos associated with the bright flares of Mrk 421 that occurred during the IC40 run, and one for excess neutrinos associated with the brightest emission periods of five other blazars (Mrk 501, 1ES 0805+524, 1ES 1218+304, 3C66A, and W Comae), all significantly fainter than the Mrk 421 flares. We find no significant excess of neutrinos from the preselected blazar directions during the selected temporal windows. We derive 90%-confidence upper limits on the number of expected flux-associated neutrinos from each search. These limits are consistent with previous point-source searches and Fermi GeV flux-correlated searches. Our upper limits are sufficiently close to the physically-interesting regime that we anticipate future analyses using already-collected data will either constrain models or yield discovery of the first blazar-associated high-energy neutrinos.

Keywords: BL Lacertae objects: general — BL Lacertae objects: individual (1ES 0806+524, 1ES 1218+304, 3C 66A, Markarian 421, Markarian 501, W Comae) — cosmic rays — gamma rays: general — neutrinos

1. INTRODUCTION

The IceCube collaboration has instrumented a cubic kilometer of Antarctic ice at the South Pole with 86 “strings” of photomultiplier tubes, readout electronics, and an internal calibration system so as to detect high-energy ($\varepsilon_\nu \gtrsim 1$ TeV) neutrinos from atmospheric cosmic ray showers and extraterrestrial sources (Achterberg et al. 2006). Operations of the 79-string and full-strength 86-string facilities since 2010 recently yielded discovery of a population of cosmic neutrinos (Aartsen et al. 2013b,a, 2014a), validating the experiment’s original motivation and approximate scale (Waxman & Bah-

call 1997; Bahcall & Waxman 2001). Given the $\gtrsim 10^\circ$ cascade-type (and less frequently, $\sim 1^\circ$ track-type) positional uncertainties and ≈ 1 per month rate of detection for the highest-confidence cosmic events, the absence of any demonstrated association with known γ -ray bursts (Aartsen et al. 2013a, 2014a,c), and the inferred near-isotropic sky distribution (Aartsen et al. 2013a), the nature of the sources of these cosmic neutrinos remains uncertain and subject to active debate (e.g., Laha et al. 2013; Anchordoqui et al. 2014a; Murase 2014; Waxman 2015).

Ultimately, identification of electromagnetic (EM)

counterparts to high-energy neutrino sources can proceed by one of two possible paths: Sufficiently variable sources may exhibit correlated variability in their neutrino and EM emissions; or sufficiently bright individual sources may (with time) be identified as *a priori* interesting, astrophysically-plausible EM sources that are coincident with a point-like or extended excess of neutrinos on the sky.

With respect to the first approach, γ -ray bursts (GRBs) have long been considered promising candidates for high-energy neutrino emission (Waxman & Bahcall 1997; Gao et al. 2013; Bustamante et al. 2015). Given the brief timescale for high-energy emission from the typical GRB, and the precision timing of IceCube-detected neutrinos, known GRBs can be readily associated with individual neutrino events even with the limited positional resolution available for the IceCube cosmic neutrinos (mostly cascade events) or associated lower-energy neutrinos that interact as track events. The relatively relaxed requirements for positional determination also allow use of the full set of detected GRBs from Swift, Fermi, the Interplanetary Network, and other satellites. In spite of this, no coincident high-energy (cascade or track) or low-energy track neutrino interactions have been found in association with any detected GRB (Abbasi et al. 2012; Adrián-Martínez et al. 2013). The inferred limit on the fraction of the cosmic neutrinos that are due to GRBs is $<1\%$ (Aartsen et al. 2014c).

Without the brief temporal window provided by GRBs, identification and confirmation of the neutrino-emitting source population(s) must depend on positional coincidence (particularly via likely-cosmic track-type events) and careful evaluation of the expected flux and spectrum under proposed theoretical models. Proposed source populations currently include star-forming galaxies (Loeb & Waxman 2006; Murase et al. 2013; Tamborra et al. 2014; Senno et al. 2015; Waxman 2015), galaxy clusters and groups (Murase et al. 2008, 2013), active galactic nuclei (AGN; Stecker et al. 1991; Halzen & Zas 1997; Atoyan & Dermer 2001; Murase et al. 2014; Tavecchio & Ghisellini 2015), and quenched-jet GRBs (Mészáros & Waxman 2001; Murase & Ioka 2013; Mészáros 2014). In addition, it remains possible that a minority of the cosmic neutrinos originate in our own Milky Way Galaxy, either via the Fermi bubbles (Crocker & Aharonian 2011; Ahlers & Murase 2014; Crocker et al. 2014; Lunardini et al. 2014), Galactic compact binary TeV γ -ray sources (Abdo et al. 2012; Anchordoqui et al. 2014b) or TeV unidentified sources (such as pulsar wind nebulae or possible hypernova remnants; Fox et al. 2013; Budnik et al. 2008). All of these scenarios are reviewed by Murase (2014).

The γ -ray bright AGN known as blazars represent

a particularly intriguing possible source population, as they are the most γ -ray luminous AGN known and the brightest extragalactic sources on the sky at TeV energies, capable of outshining all other TeV sources during some flares. Their γ -ray emission is commonly explained by invoking a leptonic scenario, in which highly-relativistic electrons in the blazar jets generate emission by a combination of synchrotron self-Compton and external inverse Compton processes. This scenario yields minimal high-energy neutrino emission.

However, if or when most of the blazars' high-energy γ -rays are produced by hadronic interactions in the relativistic jets (with a minority contribution from leptonic emission processes), the lepto-hadronic scenario, some or most of the observed γ -rays will result from cascade emission induced by γ -rays from π^0 decays. In this case, the observed TeV γ -rays will be accompanied by comparable fluxes of $\varepsilon_\nu \gtrsim 1$ TeV neutrinos from decays of coproduced π^\pm (Mannheim 1993; Gaisser et al. 1995; Böttcher 2007; Cerruti et al. 2015). In a variant of this lepto-hadronic scenario, γ -rays are produced by proton synchrotron radiation without associated high-energy neutrinos (Aharonian 2000).

In another alternative possibility, the intergalactic scenario, the γ -rays result from intergalactic cascades triggered by electron-positron pairs that are produced by ultrahigh-energy cosmic rays escaping from the sources, and photohadronic interactions with the extragalactic background light then lead to a comparable flux in high-energy γ -rays and high-energy neutrinos (Essey et al. 2010; Murase et al. 2012).

Significant neutrino emission is not anticipated in the leptonic scenario (Maraschi et al. 1992; Böttcher 2007), nor in the proton synchrotron version of the lepto-hadronic scenario. However, in a general sense we expect protons as well as electrons to be accelerated in blazar jets, and if these AGN are sources of ultrahigh-energy cosmic rays, associated high-energy neutrino emission can be detectable even if the observed γ -rays are dominated by leptonic processes (Murase et al. 2014). Carefully-designed searches for neutrino emission from the brightest blazars thus have the potential to constrain source models and important related hypotheses via either detections (possibly providing the first confirmed counterparts for any high-energy astrophysical neutrinos) or upper limits.

While leptonic models have been argued to provide a more natural fit to typical blazar spectra (Böttcher 2007), there are unresolved theoretical challenges. For example, blazar γ -ray flares can show fast variability, implying a compact emission region which is hard to reconcile with the non-observation of any high-energy cutoff from $\gamma\gamma \rightarrow e^+e^-$ (Tavecchio et al. 2011; Dermer et al. 2012). The leptonic scenario also struggles to ex-

plain the occasional “orphan” TeV blazar flares – flaring emission that is observed at TeV energies without accompanying flaring in the X-ray (Böttcher 2005; Reimer et al. 2005). Even if prototypical blazar emissions are leptonic, it is still possible that their flares (or perhaps, their orphan TeV flares) reveal a transient and variable contribution from hadronic processes. The June 2002 orphan flare of the blazar 1ES 1959+650 (Krawczynski et al. 2004; Sahu et al. 2013) is of particular note in this context. IceCube’s predecessor AMANDA-II detected a single coincident neutrino from the direction of 1ES 1959+650 during the flare, although the *a posteriori* nature of the observation has made it impossible to retrospectively assign a firm confidence level to any claim of association or non-association (Halzen & Hooper 2005; Sahu et al. 2013). Also worth noting is the recent 9.5 month-long GeV outburst of PKS B1424–418, which allowed this blazar to dominate the GeV γ -ray emissions of all catalogued blazars within the 50%-containment region of the $\varepsilon_\nu \approx 2$ PeV “HESE 35” IceCube event when that neutrino was detected, prompting the suggestion that this neutrino was emitted by PKS B1424–418 (estimated p-value of 5%; Kadler et al. 2016).

Between April 2008 and May 2009, IceCube ran in a partially-completed “IC40” 40-string configuration. The point-source analysis of this dataset found no evidence for any neutrino point sources bright enough to be distinguished above the atmospheric background (Abbasi et al. 2011b). Analysis of data gathered in IceCube’s subsequent “IC59” 59-string configuration (May 2009 to May 2010) and further searches with the full array similarly revealed no point sources, placed upper limits on the neutrino emissions of an array of candidate sources, and reported a null result for both a northern-sky time-dependent search and a Fermi-LAT flux correlated search (Aartsen et al. 2015, 2014b).

The present work extends previous point-source analyses of the IC40 data by explicitly considering the TeV γ -ray behavior of the bright northern blazars which are prime candidates for a first neutrino source detection by IceCube. Modeling the TeV lightcurves of these blazars allows us to select a set of active temporal windows and blazar directions which are (under our assumed conditions) optimal for detection of a neutrino excess over

anticipated atmospheric backgrounds. These optimized windows amount in all cases to less than 11% of the full IC40 data collection period, allowing for the possibility of discovering associated neutrino emission below the threshold of previous time-integrated searches.

Our paper proceeds as follows: We review our datasets and analysis approach in Sec. 2, and present and discuss our results in Sec. 3. We conclude and address possible future efforts in Sec. 4.

2. DATASETS AND ANALYSIS

2.1. Datasets

The IceCube 40-string dataset (hereafter IC40) was collected between April 2008 and May 2009, a total live time of 375.5 days (Abbasi et al. 2011b) during which the detector had 40 of the final 86 planned strings deployed. The data (publicly released in September 2011) records a total of 12,877 upgoing neutrino events. Extensive analyses (Abbasi et al. 2011b; Aartsen et al. 2015) have constrained the intensities of any existing point sources. The IceCube collaboration investigated the accuracy with which they could reconstruct neutrino arrival directions using the cosmic ray shadow of the moon (Aartsen et al. 2013c), and found their reconstruction uncertainty was 0.7° for the 40- and 59-string configurations.

The six blazars studied in this work are listed with their basic properties in Table 1. Publicly-available blazar data (presented in Table 2) were collected by the four-telescope Very Energetic Radiation Imaging Telescope Array System (VERITAS; Holder et al. 2006) and (for Mrk 421 historical data only) its predecessor, the Whipple Telescope (Kildea et al. 2007). Both facilities consist of atmospheric Cherenkov telescopes located at the Fred Lawrence Whipple Observatory in Arizona, yielding similar effective energy ranges of $0.1 \text{ TeV} \lesssim \varepsilon_\gamma \lesssim 30 \text{ TeV}$ (Weekes et al. 2002), with the exact limits depending on individual observation and analysis parameters such as elevation angle in the sky, analysis parameter cuts, and source spectra. All relevant blazar data are publicly available from the VERITAS website¹ Publicly-available historical TeV γ -ray data for Mrk 501 were also used².

¹ Mrk 421 long-term data (Acciari et al. 2014) are available at <http://veritas.sao.arizona.edu/veritas-science/mrk-421-long-term-lightcurve>. Data for the other blazars are from <http://veritas.sao.arizona.edu/veritas-science/veritas-blazar-spectra> and were not public at the start of this work. The data were initially provided for collaborative use and were published prior to the completion of this work.

² Mrk 501 public light curve data presented in Tluczykont et al. (2010) and available at http://astro.desy.de/gamma_astronomy/magic/projects/light_curve_archive/index_eng.html.

Table 2. Blazar Observations

Name	MJD (d)	Exp. (h)	F_{TeV}		
			Obs.	Unc.	Rev.
			$(10^{-11} \text{ cm}^{-2} \text{ s}^{-1})$		
1ES 0806+524	54564.179	0.226	2.1	1.5	...

Table 2 continued

Table 1. VERITAS Northern Blazars

Name	R.A.	Dec.	z	L_{TeV} ($10^{44} \text{ erg s}^{-1}$)	F_{TeV} ($10^{-11} \text{ cm}^{-2} \text{ s}^{-1}$)	ε_{th} (TeV)	Γ_{obs}	Γ_{src}	N_{obs}
1ES 0806+524	08:09:59.0	+52:19:00	0.138	0.1	0.2	0.3	3.6	2.7	4
1ES 1218+304	12:21:26.3	+30:11:29	0.182	1.6	1.8	0.2	3.1	2.2	20
3C 66A	02:22:41.6	+43:02:36	0.41	5.8	1.3	0.2	4.1	2.0	17
Mrk 421	11:04:19.0	+38:11:41	0.031	0.4	4.6	0.4	2.2	2.0	93
Mrk 501	16:53:52.2	+39:45:37	0.034	0.1	3.1	0.3	2.7	2.5	15
W Comae	12:21:31.9	+28:13:59	0.102	0.4	1.9	0.2	3.8	3.0	19

NOTE—Coordinates are provided in J2000; N_{obs} gives the number of observations during the IC40 observing run. Typical luminosities L_{TeV} and fluxes F_{TeV} are over $0.2 \text{ TeV} < \varepsilon_{\gamma} < 30 \text{ TeV}$. Power-law photon indices for Mrk 421 and Mrk 501 are known to be variable. The redshift of 3C 66A is uncertain, but bounded between 0.33 and 0.44. ε_{th} is the threshold energy for VERITAS observations. Γ_{obs} is the measured γ -ray spectral index, while Γ_{src} is the spectral index corrected for extragalactic background light absorption using the models of [Finke et al. \(2010\)](#) and [Inoue et al. \(2013\)](#). Blazar properties via TeVCat ([Wakely & Horan 2008](#)).

Table 2 (*continued*)

Name	MJD (d)	Exp. (h)	F_{TeV}		
			Obs. ($10^{-11} \text{ cm}^{-2} \text{ s}^{-1}$)	Unc.	Rev.
"	54566.177	2.554	−0.47	0.72	0.34
"	54567.153	0.562	1.0	1.6	...
"	54821.408	0.595	0.52	0.83	...
1ES 1218+304	54829.516	1.032	0.92	0.56	...
"	54830.524	0.869	3.11	0.67	...
"	54838.514	1.037	1.90	0.56	...
"	54839.518	0.859	2.14	0.63	...
"	54856.459	0.298	3.3	1.1	...
"	54862.454	3.072	3.79	0.37	...

NOTE—Fluxes over $0.2 \text{ TeV} < \varepsilon_{\gamma} < 30 \text{ TeV}$ (F_{TeV}) are reported as observed (Obs.) with Gaussian uncertainties (Unc.), and with forced-positive revised flux estimates (Rev.) where necessary. Derivation of revised fluxes is described in Sec. 2.2. Mrk 421 data were obtained from <http://veritas.sao.arizona.edu/veritas-science/mrk-421-long-term-lightcurve> ([Acciari et al. 2014](#)). Data for the other blazars are from <http://veritas.sao.arizona.edu/veritas-science/veritas-blazar-spectra>. Table 2 is published in its entirety in machine-readable format. A portion is shown here for guidance regarding its form and content.

2.2. TeV Lightcurves

We wish to carry out a targeted search for excess neutrinos when the monitored blazars are relatively bright in TeV γ -rays. This requires defining temporal windows of interest for each blazar. While VERITAS makes discrete measurements, the IC40 data were taken continuously, meaning that every detected neutrino must be judged either in or out of sample. We choose to make this judgment by reference to interpolated light curves, which allows us to expand the temporal windows of interest for each blazar beyond the intervals of active VERITAS observation.

This requires us to choose an interpolation approach. We find traditional linear or spline-interpolation approaches not useful, as they result in unrealistic predictions during large data gaps and also (relatedly) because they lack relevant physical underpinning. Since our primary concern is to avoid accepting neutrinos when the blazar flux is low, we seek a conservative interpolation that will revert to a low “baseline” flux in the absence of constraining data, thereby excluding these periods from our detection windows.

Moreover, given the infrequent and non-continuous nature of the γ -ray measurements, we do not find Bayesian Blocks-type approaches, as adopted for example by [Resconi et al. \(2009\)](#), to be appropriate in this case. Rather, we seek to extend observed periods of flaring and excess emission in a realistic and physically-motivated way forward and backward in time, we will be able to accept neutrinos as potential signal when they are detected close to these periods. These concerns lead us to adopt a Gaussian process regression (GPR) ([Rasmussen & Williams 2006](#)) as our interpolation approach.

Gaussian Process Regression assumes that process values are generated as a linear combination of inputs with a multivariate normal distribution described by stationary mean and covariance functions. It is a non-parametric method that fits data without choosing a specific functional form; see [Rasmussen & Williams \(2006\)](#) for details. As applied by us to VERITAS blazar observations, the GPR works in two passes. In the first pass, it analyzes the data to determine the best-fit mean and covariance “hyperparameters.” In our case, we precondition the blazar light curves, as described below, so that the mean function is zero, constant and fixed, for each blazar; hence we fit for the covariance hyperparameters only. On the second pass, the GPR uses the hyperparameters and observed data values (ignoring the uncertainties) to predict the maximum likelihood

flux (and confidence intervals on that flux) at all intermediate points. Beyond a few correlation lengths, the maximum likelihood flux reverts to the mean value, and the 90%-confidence bounds expand to encompass the full range of the observed data, illustrating the fundamentally conservative nature of this approach.

Our light curve preconditioning begins by replacing negative flux measurements, which are unphysical, with forced-positive replacement values (Table 2). These values are calculated from the associated VERITAS flux estimate and uncertainty as follows: Treating the flux estimate and uncertainty as the mean and standard deviation of a Gaussian distribution, we exclude the negative-flux portion of the distribution and use the median of the resulting positive-flux distribution as our replacement value.

Next, we calculate a “baseline flux” F_{base} for each blazar. Under the assumption that measurement uncertainties dominate systematic effects at low flux levels, and that the blazar emission consists of a dominant baseline flux supplemented by occasional periods of excess and flaring emission, we define the baseline flux for each blazar as the mode of the Gaussian kernel density estimator (KDE) for the blazar flux measurements. The KDE mode should be robust to a positive “tail” of excess and flaring emission episodes. We use the `scipy`

(Jones et al. 2001–) statistics package implementation. The resulting baseline fluxes are listed in Table 3.

In the final step of preconditioning, we divide the blazar flux measurements (and replacement values) by the baseline flux for that blazar and take the natural logarithm. Working in log-space reduces the heteroskedasticity of the flux measurements (which exhibit substantial positive excursions, but have negative excursions bounded to the physical range of non-negative fluxes), making the light curves better suited for GPR analysis. This approach allows us to set the GPR mean to a fixed constant zero for all blazars.

To carry out the GPR hyperparameter fitting and interpolation, we use the python package `pyGPs` (Neumann et al. 2014). We run the code using the squared exponential kernel with isotropic distances, Gaussian likelihood, exact inference, and a constant mean function, set to zero. The code optimizes the fit by minimizing the negative log marginal likelihood with respect to the hyperparameters. The hyperparameters for Mrk 421 and Mrk 501 were optimized using the extensive historical data. These hyperparameters were then used to generate the light curves from the data concurrent with IC40. All resulting best-fit hyperparameter values are presented in Table 3.

Table 3. Results of Gaussian Process Regression

Blazar Name	N_{obs}	F_{max}	F_{base}	Correlation		Noise	
				Time	Dev.	Dev.	NLML
		$(10^{-11} \text{ cm}^{-2} \text{ s}^{-1})$		(d)			
1ES 0806+524	4	2.1	0.6	0.14	0.81	0.10	4.47
1ES 1218+304	20	4.5	1.6	0.55	1.25	0.08	29.68
3C 66A	17	4.1	1.5	0.89	0.86	0.19	15.56
Mrk 421	93	60.6	4.4	0.61	0.99	0.07	133.96
Mrk 501	15	9.1	1.5	0.52	1.60	0.10	27.44
W Comae	19	4.8	0.5	0.99	1.63	0.10	32.05

NOTE—Interpolated curves were generated using Gaussian likelihood, exact inference, a constant mean function and a squared exponential covariance function with isotropic distances. Maximum and baseline fluxes (F_{max} , F_{base}) are over $0.2 \text{ TeV} < \varepsilon_{\gamma} < 30 \text{ TeV}$. F_{base} is the value of the mean function and was estimated as the mode of a Gaussian kernel density estimator, as applied to the complete set of observations for each source. The covariance function has two hyperparameters, the log of the correlation time and the log of the covariance noise. The likelihood function hyperparameter is the natural log of the standard deviation of the signal noise. The hyperparameters were optimized by minimizing the negative log marginal likelihood (NLML) with respect to the hyperparameters.

Blazars show variability on timescales as small as hours or even minutes. This is reflected in the correlation lengths from the GPR, which are all less than a day, implying flux measurements separated by more than a day are effectively uncorrelated. The correla-

tion length for 1ES 0806+524 was significantly shorter than the other blazars, though due to a small sample size, the value is not well constrained. Better estimates of the correlation length would require more extensive monitoring or historical data, as was used for Mrk 421

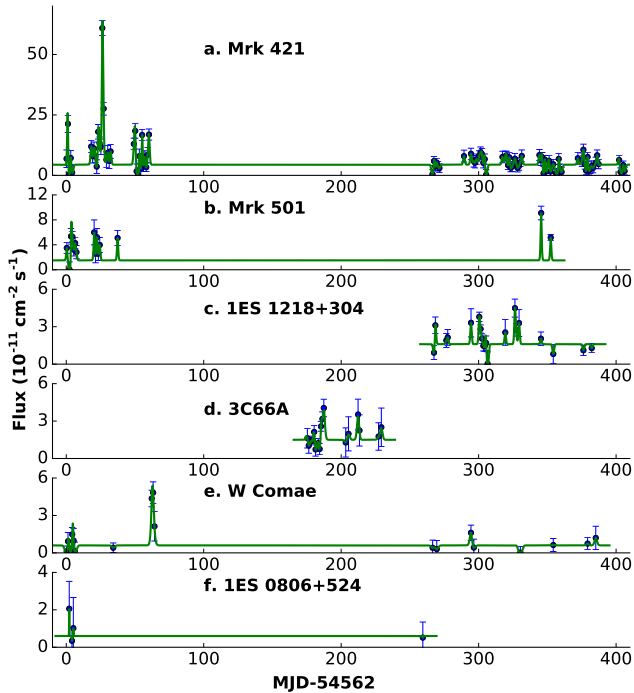


Figure 1. VERITAS TeV γ -ray light curves for six northern blazars subject to regular monitoring during the IC40 run, along with the maximum-likelihood interpolation resulting from our Gaussian process regression (Sec. 2.2). Time is in days since the start of IC40 (MJD 54562), aligned across all lightcurves.

and Mrk 501.

The resulting maximum-likelihood GPR-interpolated TeV γ -ray light curves for our six target blazars, which we generate at one hour resolution, are presented in Fig. 1. For both Mrk 501 and 1ES 1218+304, there exist short periods where the interpolated curve overshoots the measured flux points. This behavior does not impact the selection of temporal windows of interest; however, if the blazar emission did not actually increase during these intervals, then it will lead to a slight overestimation of the integrated TeV γ -ray fluence in these cases.

2.3. Analysis Approach

Before using these interpolated light curves to define (statistically optimal) temporal windows of interest for our search for an excess of associated neutrinos, we need to understand the expected rate of background atmospheric neutrinos. This requires choosing a region of interest (ROI), that is, an acceptance radius (angle) around each blazar position. IceCube has established a 0.7° uncertainty in track event reconstruction (Aartsen et al. 2013c). We treat this as the standard deviation for a two-dimensional Gaussian distribution and find that 99.5% of neutrinos should be found within a 2.3° radius of the reconstructed direction. We adopt this 2.3° radius to define the ROI for each blazar.

Selection of the temporal windows of interest begins with the observation that the background atmospheric neutrinos are distributed uniformly in time and near-uniformly on the sky (Abbasi et al. 2011b; Aartsen et al. 2015). The chief exception is the excess of events near the horizon owing to atmospheric muons from the southern hemisphere being (erroneously) reconstructed to low northern declinations. Since none of the targeted blazars have declinations $\delta_{2000} < +25^\circ$, we can safely ignore this effect. Hence, the number of background neutrinos within the 2.3° -radius ROI for any blazar is expected to follow Poisson statistics, with an expected number of 0.023 neutrinos per day (≈ 1 neutrino per ROI per 44 days). (Note that in the next section we test this assumption using Monte Carlo simulations.)

Having generated interpolated light curves in TeV γ -rays for all six monitored blazars, we use their variability to our advantage by selecting the brightest emission periods for our search, maximizing our sensitivity to flux-correlated neutrino emission in excess of the atmospheric background.

Considering the union of the six light curves at one hour resolution, we sort flux measurements (irrespective of target blazar) from brightest to faintest. This sorting yields a one-to-one mapping from any given TeV flux threshold to a corresponding total exposure time (with reduced thresholds implying greater integration times), along with an associated total integrated fluence in TeV γ -rays. The total exposure time, along with the angular size of our adopted ROI, implies an expected number of background atmospheric neutrinos, which in turn implies a minimum number of blazar-associated neutrinos which would have to be present to yield a $>3\sigma$ detection assuming zero detected atmospheric neutrinos. Our optimization is as follows: We select the flux threshold that maximizes the ratio of the integrated TeV fluence to the number of neutrinos needed for $>3\sigma$ detection.

Our prior expectation was that this optimization would yield, for the optimal flux threshold, multiple disjoint temporal acceptance windows across the brightest emission periods of several distinct blazars. In fact, however, when applied to the data for all six blazars, the optimal flux threshold yields acceptance windows totalling ≈ 46 days from Mrk 421 only, which is often the brightest blazar in the sample. These temporal windows of interest are shown in Fig. 2 and presented in Table 4. The temporal window includes 11% of the IC40 live time, and close to 18% of the live time for Mrk 421, which is close to the 3σ duty cycle calculated in Resconi et al. (2009). Though this is the optimal window as defined by our analysis, it completely omits the five remaining blazars. So we choose to carry out two distinct searches for excess neutrino emission: First, a Mrk 421-only analysis (the optimal search, according to our original search

criteria); and second, a Mrk 421-exclusive analysis using the light curves from the five other blazars. Optimization of the flux threshold for the second analysis results in a total ≈ 52 day-long acceptance window including some coverage of each of the five remaining blazars, as shown in Fig. 3 and presented in Table 4.

Table 4. Blazar Times of Interest

Name	T_{start} (d)	T_{stop} (d)
1ES 0806+524	2.138	2.221
1ES 1218+304	268.058	269.266
	276.516	277.766
	293.766	295.141
	299.766	302.849
	304.683	305.433
	318.849	319.891
	325.641	327.766
	328.599	330.099
	345.016	345.641
3C66A	179.687	180.437
	185.104	188.937
	204.979	205.937
	210.854	213.687
	227.729	230.312
Mrk 421	0.116	1.532
	3.199	3.532
	17.324	21.366
	22.616	28.241
	29.157	30.949
	31.449	33.032
	48.449	50.741
	53.116	53.616
	54.699	55.866
	56.866	57.532
	58.949	61.157
	267.574	267.824
	288.741	289.991
	293.699	295.199
	298.074	298.824
	299.907	302.866
	303.741	304.449
	316.782	317.949
	318.824	320.657
	321.949	322.616
	325.991	326.907
	330.657	331.991
	343.574	346.324
	348.241	348.449
	350.866	351.199
	358.241	358.657
	371.741	372.657
	375.199	376.991

Table 4 continued

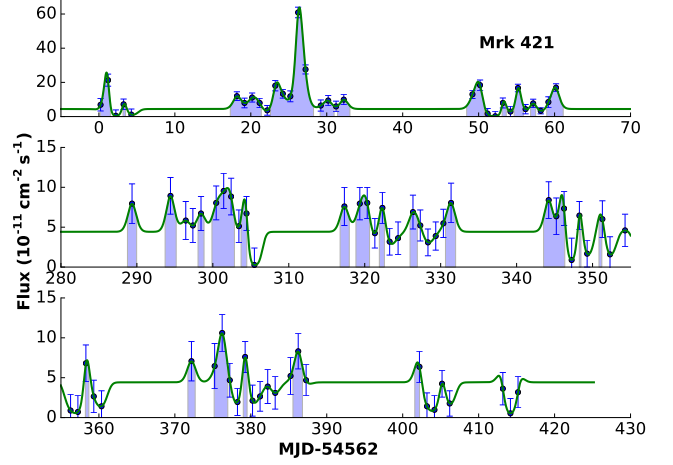


Figure 2. Times of interest for Mrk 421 (shaded intervals). These times were selected in our initial optimization as the most sensitive search for associated neutrinos (Sec. 2.3). The selection includes 45.6 days with a total TeV γ -ray fluence of 4.1×10^{-4} photons cm^{-2} and yields an expected background of 1.03 neutrinos.

Table 4 (continued)

Name	T_{start} (d)	T_{stop} (d)
	379.032	379.532
	385.574	386.782
	401.616	402.199
Mrk 501	−0.961	0.830
	3.247	8.289
	18.705	25.789
	35.872	38.83
	343.872	347.122
	350.955	353.914
W Comae	4.494	5.036
	61.411	64.327

NOTE—Start and stop times (T_{start} , T_{stop}) for the temporal windows of interest are reported in days since the start of the IC40 run (i.e., MJD−54562). Temporal windows for two distinct searches are reported, one using Mrk 421 data only (Mrk 421-only) and one using only data from other blazars (Mrk 421-exclusive); see text for details.

2.4. Monte Carlo Simulations

We carry out Monte Carlo (MC) simulations to confirm our understanding of the atmospheric neutrino background. Each simulation begins by shuffling the complete list of IC40 neutrino detections, associating each original neutrino ν_i with another randomly-selected neutrino ν_j . In our MC scrambling, the neutrino ν_i retains its original declination and receives the original

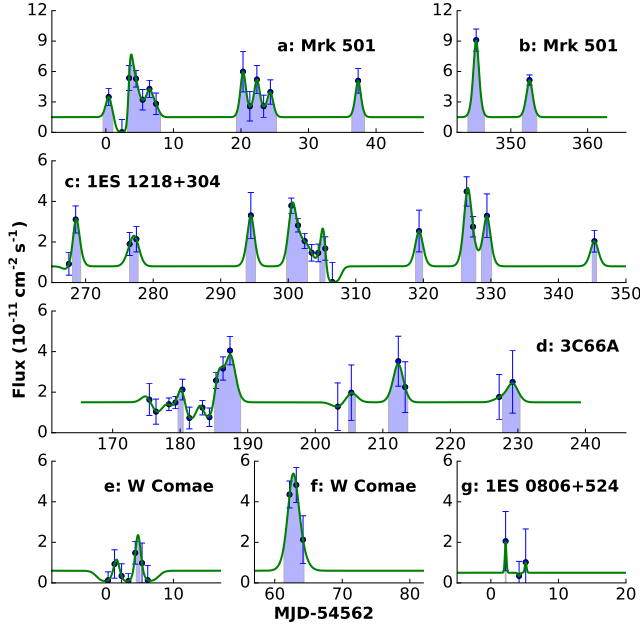


Figure 3. Times of interest for Mrk 501, 1ES 1218+304, 3C 66A, W Comae, and 1ES 0806+524 resulting from our Mrk 421-exclusive search (shaded intervals). These times were selected as the most sensitive search for associated neutrinos that excludes data from Mrk 421 (Sec. 2.3). The selection includes 51.6 days with a total γ -ray fluence of 1.4×10^{-4} photons cm^{-2} and yields an expected background of 1.17 neutrinos.

arrival time of neutrino ν_j , with its new right ascension derived by adjusting the original right ascension for the difference in local sidereal time between the original and new arrival times. In this way, each neutrino retains its original arrival direction with respect to the physical IC40 array. Applying this procedure leads to a new scrambled dataset that retains the original integrated distributions in time, declination, and arrival direction, while scrambling neutrino positions quasi-randomly in right ascension.

We produce 10,000 MC datasets and search for neutrinos arriving during the predefined ROIs and temporal windows. We then use these results to verify the expected arrival rate and assumption of Poisson behavior for the background atmospheric neutrinos.

Our Mrk 421-only search uses a flux cutoff accepting each lightcurve point brighter than $6.22 \times 10^{-11} \text{ cm}^{-2} \text{ s}^{-1}$, accounting for 45.6 days in total. The integrated fluence during this temporal window is $4.1 \times 10^{-4} \text{ cm}^{-2}$. From the IC40 data, an average of 1.03 neutrinos should arrive within the 2.3° -radius ROI during the 45.6 days. The 10,000 MC data sets show a Poisson background with a mean of 1.03 and a variance of 1.01. Thus, a $>3\sigma$ detection would require ≥ 5 neutrinos during the temporal acceptance window.

Our Mrk 421-exclusive search uses a flux cutoff of $1.88 \times 10^{-11} \text{ cm}^{-2} \text{ s}^{-1}$, with 51.6 days above this level,

and an integrated fluence of $1.4 \times 10^{-4} \text{ cm}^{-2}$. IC40 data predicts the ROI should see an average of 1.17 neutrinos during the temporal windows. The 10,000 scrambles demonstrated a Poisson background with a mean and a variance of 1.10. Detection at $>3\sigma$ would hence require ≥ 6 neutrinos.

3. RESULTS AND DISCUSSION

In order to derive physical constraints from our observations, we need to derive expected IC40 neutrino detection rates from the observed TeV γ -ray fluxes of the targeted blazars, using an appropriate model.

We adopt a standard lepto-hadronic model for this purpose. The measured TeV photon fluence for each blazar can be expressed as the integral of the differential spectrum:

$$\phi_i = \int_{\varepsilon_{\text{th}}}^{\varepsilon_2} \frac{N_0}{\varepsilon_\gamma^2} \left(\frac{\varepsilon_\gamma}{1 \text{ TeV}} \right)^{2-\Gamma_{\text{obs},i}} d\varepsilon_\gamma \quad (1)$$

where ε_γ is the γ -ray energy, ε_{th} is the threshold energy for that blazar, $\varepsilon_2 = 30 \text{ TeV}$ is the upper energy limit of VERITAS, $\Gamma_{\text{obs},i}$ is the observed power-law photon index for each blazar (Table 1), and N_0 is a normalization constant. Once N_0 is known for each blazar, the differential spectrum for neutrinos can be calculated. The number of expected neutrinos is the integral of the neutrino spectrum times the effective area of IC40:

$$N_{\text{exp},i} = \int_{\varepsilon_1}^{\varepsilon_2} \frac{N_0}{4 \varepsilon_\nu^2} \left(\frac{\varepsilon_\nu}{0.5 \text{ TeV}} \right)^{2-\Gamma_{\text{src},i}} A_{\text{IC40}}(\varepsilon_\nu) d\varepsilon_\nu \quad (2)$$

where N_0 is a constant calculated in Eq. 1, ε_ν is the neutrino energy, ε_1 and ε_2 bound the calculation over the IC40 effective area $A_{\text{IC40}}(\varepsilon_\nu)$ as presented in Abbasi et al. (2011a), and $\Gamma_{\text{src},i}$ is the blazar spectral index after correcting for γ -ray absorption by the extragalactic background light using the models of Finke et al. (2010) and Inoue et al. (2013) (Table 1). If $N_{\text{exp},i}$ is larger than the calculated upper limit, non-observation will constrain the fraction of γ -rays produced in lepto-hadronic interactions.

Our Mrk 421-only search yields no neutrinos during the temporal acceptance windows, while ≥ 5 were required for a detection claim. Our non-detection implies an upper limit of 1.27 (2.30 in total, minus 1.03 background) flux-associated neutrinos from Mrk 421 at 90%-confidence. If the TeV γ -ray flux from Mrk 421 during our identified periods of excess and flaring emission were entirely due to hadronic interactions, this would give 0.79 neutrinos. As this is smaller than the upper limit, we cannot constrain the hadronic process for Mrk 421; the relevant figure of merit is $N_{\nu,\text{obs}}/N_{\nu,\text{exp}} < 1.6$.

Our Mrk 421-exclusive search yields one neutrino during the joint acceptance windows for the remaining five blazars; ≥ 6 neutrinos were required in this case for

$>3\sigma$ detection. The neutrino arrives from the Mrk 501-specific ROI with an angular offset of 1.5° at MJD 54562.71 (time 0.71 in Figure 3 and Table 4). With one detected neutrino, we have an upper limit of 2.79 (3.89 total minus 1.10 background) neutrinos at 90%-confidence. Applying our hadronic interaction model to the identified periods of excess and flaring emission from these blazars leads to an expectation of 0.02 neutrinos over the joint acceptance windows with $N_{\nu,\text{obs}}/N_{\nu,\text{exp}} < 140$ as the figure of merit. Note that while the integrated γ -ray fluence from Mrk 421 was roughly three times larger than the fluence from the other five blazars, its expected neutrino fluence was nearly 35 times larger. This is due to the hardness of Mrk 421's spectrum, which yields more neutrinos at higher energies where IceCube is more sensitive. The five other blazars (excepting 3C 66A, which had a much smaller integrated fluence) had softer spectra, yielding more neutrinos at lower energies where IceCube is less sensitive.

A previously published IC40 analysis (Abbasi et al. 2011b) for Mrk 421 identified and observed two neutrinos, consistent with background, with theoretical neutrino flux calculations yielding a best fit of 2.6 signal events, producing a differential flux limit of $dN/dE \leq 11.71 \times 10^{-12} \text{ TeV}^{-1} \text{ cm}^{-2} \text{ s}^{-1}$ for muon neutrinos. Additional searches (Aartsen et al. 2014b) continue to show no correlated neutrinos. Independent analysis of Mrk 421 using γ -ray data from Fermi (Petropoulou et al. 2016) showed that focusing on blazar flares may be optimal for discovery of correlated $>\text{PeV}$ neutrinos.

While our limits do not suffice to constrain our chosen hadronic interaction model for these blazars, the existence of an additional seven years' worth of IceCube data, all taken with greater-volume configurations of the detector (including five years' worth of data using all 86 strings), is encouraging. This should amount to roughly 14 times the effective integration of one year of IC40 data and, in the event of a nondetection, reduce the figure of merit by a factor of ≈ 3.8 . Hence, unless the variability and flaring properties of Mrk 421 and the remaining blazars during IC40 were in some way unusual, we anticipate being able to constrain hadronic models for Mrk 421 with data already in hand at both IceCube and VERITAS, with the anticipated figure of merit (in the case of nondetection) being $N_{\nu,\text{obs}}/N_{\nu,\text{exp}} \lesssim 0.4$. Similarly but less conclusively, we anticipate being able to make a much more sensitive (although potentially, not yet physically constraining) search for excess flux-associated neutrinos from Mrk 501 and the other northern blazars, with $N_{\nu,\text{obs}}/N_{\nu,\text{exp}} \lesssim 32$ as the anticipated figure of merit in the case of non-detection.

4. CONCLUSIONS

We defined a search for TeV γ -ray flux-correlated neutrinos from six bright northern blazars. The search used publicly-available neutrino data from the IceCube 40-string "IC40" observing run and public TeV γ -ray data from VERITAS. Interpolating the VERITAS light curves with a Gaussian process regression, we isolated temporal windows of interest for two searches: a Mrk 421-only search and a Mrk 421-exclusive search. We confirmed the Poisson behavior of the near-isotropic background with a Monte Carlo simulation using scrambled neutrino datasets.

Our Mrk 421-only search found zero neutrinos compared to a background expectation of 1.03 neutrinos and a requirement of ≥ 5 neutrinos for a $>3\sigma$ detection claim, while our Mrk 421-exclusive search found one neutrino compared to a background expectation of 1.1 neutrinos and a requirement of ≥ 6 neutrinos for a $>3\sigma$ detection claim.

Both findings are consistent with background expectations, yet they are also consistent with expectations from hadronic blazar models. These non-detections place upper limits of 1.27 neutrinos for Mrk 421 (with a figure of merit $N_{\nu,\text{obs}}/N_{\nu,\text{exp}} < 1.6$) and 2.79 neutrinos for the five other blazars (figure of merit $N_{\nu,\text{obs}}/N_{\nu,\text{exp}} < 140$). These limits are not strong enough to place constraints on the hadronic process for any of the blazars, though the figure of merit for Mrk 421 is close to being physically constraining. However, this search was limited to only the IC40 dataset. The methods developed in Sec. 2.3 work equally well for any additional existing data. An interesting future project would be to extend this search to more recent public datasets.

Our analysis showed that Mrk 421 dominates the TeV γ -ray flux from the northern blazars. Mrk 421 is currently monitored in the TeV on a daily or near-daily basis by the High-Altitude Water Cherenkov (HAWC; DeYoung & HAWC Collaboration 2012) and First Cherenkov Telescope using a G-APD Camera for TeV Gamma-ray Astronomy (FACT; Anderhub et al. 2010) facilities. Since IceCube has been operating at full strength since 2011, it may be fruitful to perform a flux-correlated search on Mrk 421, as even a non-detection will reduce the figure of merit, potentially to a physically constraining value.

As mentioned in Sec. 1, TeV orphan flares are a particular candidate for the dominance of hadronic acceleration processes. Using hard X-ray data from the Swift BAT all-sky monitor (Krimm et al. 2013) in tandem with HAWC, FACT, and VERITAS data, TeV γ -ray orphan flares could be isolated from other periods of high TeV flux and used for a distinct, focused search for associated neutrinos.

The authors acknowledge support from the Eberly College of Science, the Penn State Institute for Gravitation and the Cosmos, and the partner collaborations of the Astrophysical Multimessenger Observatory Network (AMON). The authors would like to thank M. Errando, E. Pueschel, and S. O’Brien from the VERITAS collaboration for their efforts in preparing and publishing the blazar light curves. The authors acknowledge

statistical consulting support from Prof. B. Shaby of the Penn State Department of Statistics. This work was supported in part by the National Science Foundation under Grant Number PHY-1412633.

Facilities: IceCube, VERITAS, Whipple Telescope

Software: SciPy (Jones et al. 2001–), NumPy (van der Walt et al. 2011), pyGPs (Neumann et al. 2014), matplotlib (Hunter 2007)

REFERENCES

- Aartsen, M. G. et al. 2013a, *Science*, 342, 1
 — 2013b, *Physical Review Letters*, 111, 021103
 — 2013c, *ArXiv.org*, 1305.6811
 — 2015, *ApJ*, 807, 46
 — 2014a, *Physical Review Letters*, 113, 101101
 — 2014b, *ApJ*, 796, 109
 — 2014c, *ArXiv.org*, 1412.6510
 Abbasi, R. et al. 2012, *Nature*, 484, 351
 — 2011a, *PhRvD*, 84, 082001
 — 2011b, *ApJ*, 732, 18
 Abdo, A. A. et al. 2012, *ApJ*, 753, 159
 Acciari, V. A. et al. 2014, *Astroparticle Physics*, 54, 1
 Achterberg, A. et al. 2006, *Astroparticle Physics*, 26, 155
 Adrián-Martínez, S. et al. 2013, *A&A*, 559, A9
 Aharonian, F. A. 2000, *NewA*, 5, 377
 Ahlers, M. & Murase, K. 2014, *PhRvD*, 90, 023010
 Anchordoqui, L. A. et al. 2014a, *Journal of High Energy Astrophysics*, 1, 1
 Anchordoqui, L. A., Goldberg, H., Paul, T. C., da Silva, L. H. M., & Vlcek, B. J. 2014b, *PhRvD*, 90, 123010
 Anderhub, H. et al. 2010, *ArXiv.org*, 1010.2397
 Atoyan, A. & Dermer, C. D. 2001, *Physical Review Letters*, 87, 221102
 Bahcall, J. & Waxman, E. 2001, *PhRvD*, 64, 023002
 Böttcher, M. 2005, *ApJ*, 621, 176
 — 2007, *Ap&SS*, 309, 95
 Budnik, R., Katz, B., MacFadyen, A., & Waxman, E. 2008, *ApJ*, 673, 928
 Bustamante, M., Baerwald, P., Murase, K., & Winter, W. 2015, *Nature Communications*, 6, 6783
 Cerruti, M., Zech, A., Boisson, C., & Inoue, S. 2015, *MNRAS*, 448, 910
 Crocker, R. M. & Aharonian, F. 2011, *Physical Review Letters*, 106, 101102
 Crocker, R. M., Bicknell, G. V., Carretti, E., Hill, A. S., & Sutherland, R. S. 2014, *ApJL*, 791, L20
 Dermer, C. D., Murase, K., & Takami, H. 2012, *ApJ*, 755, 147
 DeYoung, T. & HAWC Collaboration 2012, *Nuclear Instruments and Methods in Physics Research A*, 692, 72
 Essey, W., Kalashev, O. E., Kusenko, A., & Beacom, J. F. 2010, *Physical Review Letters*, 104, 141102
 Finke, J. D., Razzaque, S., & Dermer, C. D. 2010, *ApJ*, 712, 238
 Fox, D. B., Kashiyama, K., & Mészáros, P. 2013, *ApJ*, 774, 74
 Gaisser, T. K., Halzen, F., & Stanev, T. 1995, *PhR*, 258, 173
 Gao, S., Kashiyama, K., & Mészáros, P. 2013, *ApJL*, 772, L4
 Halzen, F. & Hooper, D. 2005, *Astroparticle Physics*, 23, 537
 Halzen, F. & Zas, E. 1997, *ApJ*, 488, 669
 Holder, J. et al. 2006, *Astroparticle Physics*, 25, 391
 Hunter, J. D. 2007, *Computing In Science & Engineering*, 9, 90
 Inoue, Y., Inoue, S., Kobayashi, M. A. R., Makiya, R., Niino, Y., & Totani, T. 2013, *ApJ*, 768, 197
 Jones, E., Oliphant, T., Peterson, P., et al. 2001–, *SciPy: Open source scientific tools for Python*, [Online; accessed 2016-07-26]
 Kadler, M. et al. 2016, *ArXiv.org*, 1602.02012
 Kildea, J. et al. 2007, *Astroparticle Physics*, 28, 182
 Krawczynski, H. et al. 2004, *ApJ*, 601, 151
 Krimm, H. A. et al. 2013, *ApJS*, 209, 14
 Laha, R., Beacom, J. F., Dasgupta, B., Horiuchi, S., & Murase, K. 2013, *PhRvD*, 88, 043009
 Loeb, A. & Waxman, E. 2006, *JCAP*, 5, 3
 Lunardini, C., Razzaque, S., Theodoseou, K. T., & Yang, L. 2014, *PhRvD*, 90, 023016
 Mannheim, K. 1993, *PhRvD*, 48, 2408
 Maraschi, L., Ghisellini, G., & Celotti, A. 1992, *ApJL*, 397, L5
 Mészáros, P. 2014, *Nuclear Physics B Proceedings Supplements*, 256, 241
 Mészáros, P. & Waxman, E. 2001, *Physical Review Letters*, 87, 171102
 Murase, K. 2014, *ArXiv.org*, 1410.3680
 Murase, K., Ahlers, M., & Lacki, B. C. 2013, *PhRvD*, 88, 121301
 Murase, K., Dermer, C. D., Takami, H., & Migliori, G. 2012, *ApJ*, 749, 63
 Murase, K., Inoue, S., & Nagataki, S. 2008, *ApJL*, 689, L105
 Murase, K., Inoue, Y., & Dermer, C. D. 2014, *PhRvD*, 90, 023007
 Murase, K. & Ioka, K. 2013, *Physical Review Letters*, 111, 121102
 Neumann, M., Huang, S., Marthaler, D., & Kersting, K. 2014, *pyGPS: A Package for Gaussian Processes*, [Online; accessed 2016-07-26]
 Petropoulou, M., Coenders, S., & Dimitrakoudis, S. 2016, *Astroparticle Physics*, 80, 115
 Rasmussen, C. E. & Williams, C. K. I. 2006, *Gaussian processes for machine learning* (Cambridge, Mass: MIT Press)
 Reimer, A., Böttcher, M., & Postnikov, S. 2005, *ApJ*, 630, 186
 Resconi, E., Franco, D., Gross, A., Costamante, L., & Flaccomio, E. 2009, *A&A*, 502, 499
 Sahu, S., Oliveros, A. F. O., & Sanabria, J. C. 2013, *PhRvD*, 87, 103015
 Senno, N., Mészáros, P., Murase, K., Baerwald, P., & Rees, M. J. 2015, *ApJ*, 806, 24
 Stecker, F. W., Done, C., Salamon, M. H., & Sommers, P. 1991, *Physical Review Letters*, 66, 2697
 Tamborra, I., Ando, S., & Murase, K. 2014, *JCAP*, 9, 43
 Tavecchio, F., Becerra-Gonzalez, J., Ghisellini, G., Stamerra, A., Bonoli, G., Foschini, L., & Maraschi, L. 2011, *A&A*, 534, A86
 Tavecchio, F. & Ghisellini, G. 2015, *MNRAS*, 451, 1502
 Tluczykont, M., Bernardini, E., Satalecka, K., Clavero, R., Shayduk, M., & Kalekin, O. 2010, *A&A*, 524, A48
 van der Walt, S., Colbert, S. C., & Varoquaux, G. 2011, *Computing in Science Engineering*, 13, 22
 Wakely, S. P. & Horan, D. 2008, *International Cosmic Ray Conference*, 3, 1341
 Waxman, E. 2015, *ArXiv.org*, 1511.00815

Waxman, E. & Bahcall, J. 1997, Physical Review Letters, 78,
2292

Weekes, T. C. et al. 2002, Astroparticle Physics, 17, 221